A STUDY ON M100 (NGC 4321)

Munagala Reddy Charan Reddy
Department of Physics and Astronomy
University of Bologna
Bologna, Italy, 40129.

Sarthak Nayak
Department of Physics and Astronomy
University of Bologna Bologna, Italy, 40129.

Abstract—**This paper explores advanced imaging and analysis techniques in modern interferometry, emphasizing spectrometers, deconvolution methods, and the derivation of moment images and star formation rates (SFR). Spectrometers split the passband into narrow frequency ranges for simultaneous power measurements, enhancing sensitivity and uv coverage in continuum imaging through Multi-Frequency Synthesis (MFS). Spectral line observations yield three-dimensional data cubes, crucial for studying the gas content in astronomical objects. Deconvolution, particularly the CLEAN algorithm, iteratively refines images by removing sidelobes caused by incomplete uv sampling. The generation of moment 0 (intensity) and moment 1 (velocity) images facilitates the measurement of integrated flux densities and gas surface densities, with uncertainties derived from rms noise in line-free channels. Additionally, the paper examines the Kennicutt-Schmidt law, linking gas surface density to star formation rate surface density, providing insights into the processes driving star formation in galaxies. This comprehensive approach highlights the significance of precise imaging and robust analysis in understanding astronomical phenomena.**

I. INTRODUCTION

Interferometry has revolutionized the field of astronomy, enabling high-resolution imaging of celestial objects by combining signals from multiple telescopes. This technique leverages the principles of interference to construct detailed images that surpass the resolution limits of individual telescopes. The advancements in interferometric techniques have been particularly significant with the advent of modern spectrometers and sophisticated data analysis methods.

The primary objective of this paper is to delve into the advanced imaging and analysis techniques employed in modern interferometry. We aim to provide a comprehensive understanding of how spectrometers, deconvolution techniques, moment images, and the derivation of star formation rates (SFR) contribute to an enhanced understanding of astronomical phenomena.

Spectrometers play a crucial role in modern interferometry by dividing the passband into narrow frequency ranges, allowing for simultaneous power measurements across multiple channels. This capability is vital for both continuum and spectral line observations, offering improved sensitivity and resolution. The use of large bandwidth receivers and Multi-Frequency Synthesis (MFS) further enhances the sensitivity and uv coverage in continuum imaging, enabling more detailed and accurate observations.

In spectral line observations, the generation of threedimensional data cubes provides a wealth of information about the gas content in astronomical objects. However, these observations pose challenges, such as continuum emission, which can complicate data interpretation. Techniques such as channel averaging and continuum subtraction are employed to mitigate these challenges and improve the clarity of the data.

Deconvolution techniques, particularly the CLEAN algorithm, are essential for refining interferometric images. The CLEAN algorithm iteratively removes sidelobes caused by incomplete uv sampling, resulting in clearer and more accurate images. Effective deconvolution relies on careful selection of parameters like pixel and image size, and advanced methods offer additional improvements in image quality.

Moment images, including moment 0 (intensity) and moment 1 (velocity) images, are crucial for measuring integrated flux densities and gas surface densities. These images provide valuable insights into the distribution and dynamics of gas in galaxies. Additionally, calculating uncertainties in moment images helps ensure the accuracy and reliability of these measurements.

The Kennicutt-Schmidt law, which relates gas surface density to star formation rate surface density, is a fundamental tool for understanding star formation processes. By applying this law to observational data, we can gain insights into the factors driving star formation in galaxies. Case studies and practical examples will illustrate the application of these techniques in real astronomical observations.

II. SPECTROMETERS IN INTERFEROMETRY

Spectrometers are indispensable tools in modern interferometry, providing the capability to divide the incoming electromagnetic signal into narrow frequency channels. This division enhances the ability to analyze the spectral properties of astronomical sources with high precision. Spectrometers enable simultaneous power measurements across multiple frequency channels, significantly improving both sensitivity and resolution in astronomical observations.

In interferometry, the signal from each telescope is converted into a frequency spectrum using a spectrometer. This process involves dividing the passband into N narrow frequency channels, each with a width $\Delta\nu$. The resulting data is a set of power measurements P_i for each channel i, where i= 1,2,...,N. The sensitivity of the measurements improves with the number of channels, allowing for detailed analysis of the spectral line features.

The resolution of the spectrometer is defined by its ability to distinguish between closely spaced frequency components. This resolution is given by:

$$\Delta\nu = \frac{\nu}{R} \quad (1)$$

where ν is the central frequency of the passband, and R is the resolving power of the spectrometer. Higher resolving power corresponds to narrower frequency channels and thus finer spectral resolution.

In the context of continuum imaging, spectrometers play a critical role by enabling Multi-Frequency Synthesis (MFS). MFS combines data from multiple frequency channels to improve the uv coverage and sensitivity of the interferometric image. This technique allows for more accurate reconstruction of the source structure, enhancing the quality of the final image.

The integration of spectrometers with large bandwidth receivers has further revolutionized continuum imaging. These receivers can capture a wide range of frequencies simultaneously, and when combined with MFS, they provide unprecedented sensitivity and resolution. The enhanced uv coverage achieved through MFS leads to more detailed and accurate observations of celestial sources.

Spectral line observations benefit immensely from the use of spectrometers. These observations produce three dimensional data cubes, with two spatial dimensions and one spectral dimension. The spectral dimension provides crucial information about the velocity and distribution of gas in astronomical objects. However, the presence of strong continuum emission can pose challenges in interpreting spectral line data.

To address these challenges, techniques such as channel averaging and continuum subtraction are employed. Channel averaging reduces noise by averaging the signal over several channels, while continuum subtraction involves removing the continuum emission from the spectral data. These techniques help to isolate the spectral line features, making the data more interpretable.

In summary, spectrometers are essential components of modern interferometric systems, enhancing both continuum and spectral line observations. Their ability to divide the passband into narrow frequency channels and provide simultaneous power measurements significantly improves the sensitivity and resolution of astronomical observations. The integration of spectrometers with advanced techniques like MFS and continuum subtraction further enhances the quality of interferometric data, leading to more detailed and accurate insights into the nature of celestial sources.

III. DATA ACQUISITION AND CONTINUUM IMAGING

Modern interferometric observations rely on large bandwidth receivers to capture a broad range of frequencies. These receivers enhance the sensitivity of the observations and allow the capture of more information within a shorter observation time. Multi-Frequency Synthesis (MFS) is a technique used to combine data from multiple frequency channels to create a single high-sensitivity continuum image.The primary advantage of MFS is its ability to improve the uv coverage, which in turn enhances the image quality and resolution. In MFS, the data from different frequency channels are combined. The observed visibility data V (u,v,ν) at different frequencies ν are used to reconstruct the sky brightness distribution I(l,m). The relationship between the visibility data and the sky brightness is given by the Fourier transform:

$$V(u,v,\nu) = \int\int I(l,m)\, e^{-2\pi i(ul+vm)}\, dl\, dm$$

By combining data from multiple frequencies, MFS increases the signal-to-noise ratio (SNR) of the resulting image. The noise in the combined image is reduced because it integrates the signal over a wider bandwidth. The uv plane coverage is significantly improved because different frequency channels correspond to different uv spacings. This results in better sampling of the uv plane, which is essential for accurate image reconstruction. The MFS technique is implemented in imaging software such as CASA (Common Astronomy Software Applications). The process involves several steps, including data calibration, frequency-dependent weighting, and image reconstruction.

$$I_{\text{MFS}}(l,m) = \sum_{i=1}^{N_\nu} w_i \cdot I_{\nu_i}(l,m)$$

where $I_{\nu_i}(l,m)$ is the image at frequency ν_i and w_i are the weights assigned to each frequency channel.

IV. SPECTRAL LINE OBSERVATIONS

Spectral line observations produce three-dimensional data cubes, with axes corresponding to right ascension (RA), declination (DEC), and frequency (or velocity). Each plane of the cube represents an image at a specific frequency. The data cube I(x,y,v) provides a detailed view of the spatial distribution of emission at different frequencies. This allows astronomers to study the kinematics and physical conditions of the emitting gas:

I(x,y,v)

By converting frequency to velocity using the Doppler effect, the data cube can reveal the velocity structure of the observed object:

$$v = c\left(\frac{\nu_0 - \nu}{\nu_0}\right)$$

where v is the velocity, c is the speed of light, ν_0 is the rest frequency of the spectral line, and ν is the observed frequency. Continuum emission from the target or background sources can complicate the detection and analysis of spectral lines. Accurate subtraction of the continuum is necessary to isolate the line emission. Spectral line observations often have lower signal-to-noise ratios compared to continuum observations due to the narrower bandwidth of the line channels. Increasing the observation time or using more sensitive instruments can mitigate this issue.

To improve the analysis, channel averaging can be employed when full spectral resolution is not needed. Averaging adjacent channels can improve the SNR by reducing noise:

$$I_{\text{avg}}(x,y) = \frac{1}{N}\sum_{i=1}^{N} I(x,y,\nu_i)$$

where N is the number of channels being averaged. To isolate the spectral line emission, a model of the continuum emission is created using channels free of line emission. This model is then subtracted from the data cube:

$$I_{\text{line}}(x,y,\nu) = I_{\text{total}}(x,y,\nu) - I_{\text{cont}}(x,y,\nu)$$

where $I_{\text{line}}(x,y,v)$ is the line emission, $I_{\text{total}}(x,y,v)$ is the total observed emission, and $I_{\text{cont}}(x,y,v)$ is the modeled continuum emission

V. MOMENT IMAGES

A. Moment 0 (Intensity) Images
Moment 0 images represent the total intensity of emission integrated over all velocity channels for each pixel. Mathematically, the intensity I in a Moment 0 image is given by:

$$I(x,y) = \sum_{v} S(x,y,v)\Delta v \quad (2)$$

where S(x,y,v) is the intensity as a function of spatial coordinates (x,y) and velocity v, and Δv is the channel width

in velocity space. These images are crucial for understanding the distribution of gas within a region, providing a two-dimensional map of the total emission from the source.
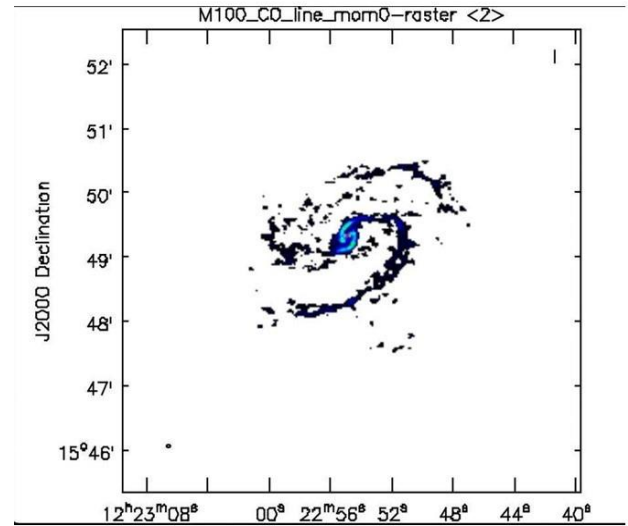

Fig. 1. Moment 0 images, also known as integrated intensity maps, are generated by summing the flux density over all channels along the spectral axis for each spatial pixel in a data cube. This provides a measure of the total emission (integrated flux) at each position in the image.

Significance
- **Gas Distribution**: Moment 0 images are used to map the distribution of gas (e.g., HI, CO) in galaxies and other astronomical objects.
- **Total Emission:** They represent the total emission from the observed region, providing a way to quantify the amount of emitting material.
- **Star Formation:** These images help in identifying regions with high gas concentrations, which are potential sites for star formation.

B. Moment 1 (Velocity) Images
Moment 1 images, also known as intensity-weighted velocity maps, show the average velocity of the gas along the line of sight. The velocity v_{avg} at each pixel is calculated as:

$$v_{\text{avg}}(x,y) = \frac{\sum_v v \cdot S(x,y,v)}{\sum_v S(x,y,v)} \quad (3)$$

where v is the velocity, and S(x,y,v) is the intensity at each velocity channel. These images are useful for studying the kinematics of the gas, including rotation, inflows, outflows, and other dynamic processes.
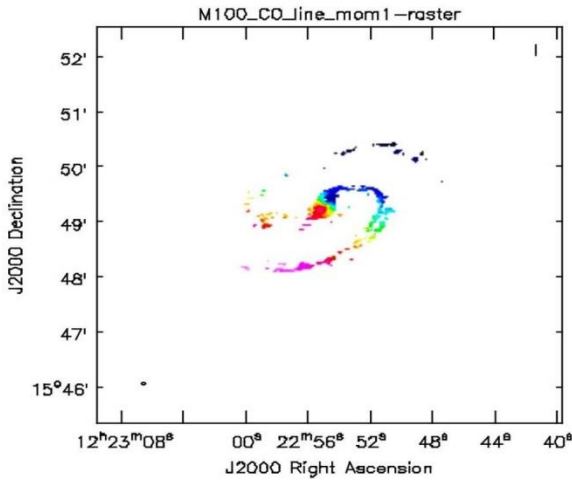
Fig. 2. Moment 1 image, or intensity-weighted mean velocity maps, show the average velocity of emitting material along the line of sight for each spatial pixel. This is achieved by weighing each velocity channel by its intensity before averaging.

Significance

- **Kinematics:** Moment 1 images are crucial for studying the kinematics of galaxies, including rotation curves and velocity dispersions.
- **Dynamical Information:** They provide insights into the motion of gas within galaxies, such as inflows, outflows, and rotational dynamics.
- **Turbulence and Flows:** These images help identify regions with turbulent motions, streaming flows, or other kinematic features.

C. Measurement of Integrated Flux Densities
Integrated flux density is measured from Moment 0 images by summing the intensity values over a defined region. The integrated flux density F_{int} is given by:

$$F_{int} = \sum_{x,y} I(x,y) \qquad (4)$$

This measurement is typically calibrated to physical units (e.g., Jy km/s) using appropriate factors. This method provides a direct measure of the total emission from a region, allowing for the calculation of gas mass and other physical properties.

D. Uncertainty Calculations
The uncertainty in moment images arises from the noise in the data and the number of channels over which the integration is performed. For Moment 0 images, the uncertainty σ_{mom0} is estimated as:

$$\sigma_{mom0} = rms \times \sqrt{N_{chan}} \times \Delta v \qquad (5)$$

where rms is the root mean square noise in line-free channels, N_{chan} is the number of channels, and Δv is the channel width.

For Moment 1 images, the uncertainty involves propagating the errors from the intensity-weighted velocities:

$$\sigma_{v_{avg}} = \sqrt{\frac{\sum_v (v - v_{avg})^2 \cdot S(x,y,v)}{\sum_v S(x,y,v)}} \qquad (6)$$

VI. STAR FORMATION RATES (SFR)

A. Kennicutt-Schmidt Law
The Kennicutt-Schmidt law quantifies the relationship between the gas surface density (Σ_{gas}) and the star formation rate surface density (Σ_{SFR}) in galaxies. The law is expressed as:

$$\Sigma SFR = A(\Sigma gas)N \qquad (7)$$

where A is a normalization constant, and N is the power law index, typically around 1.4. This indicates that regions with higher gas densities tend to have higher star formation rates.

B. Relationship Between Gas Surface Density and SFR
In the context of M100, the relationship between gas surface density and SFR can be analyzed by comparing maps of molecular gas (e.g., CO observations) with star formation tracers (e.g., Hα or infrared emission). Practical examples from M100 show that regions with enhanced molecular gas densities, such as the spiral arms, exhibit higher star formation rates, consistent with the Kennicutt Schmidt law.

For instance, if the surface density of molecular gas in a region of M100 is measured to be $\Sigma_{gas} = 50 M_\odot pc^{-2}$, and the constants A and N are known from empirical studies
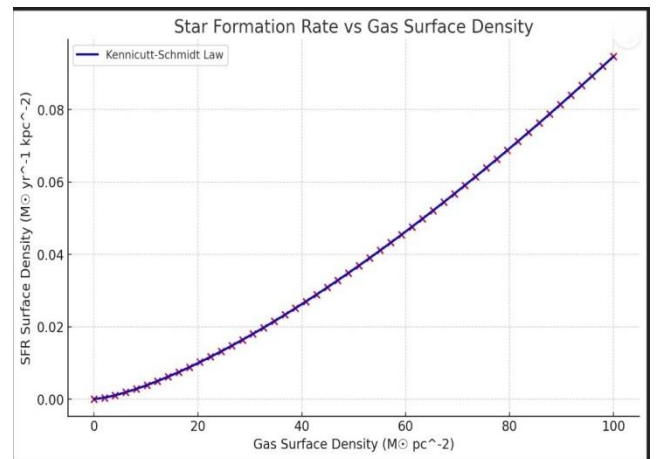

Fig. 3. The Star Formation Rate (SFR) graph presented here illustrates the relationship between gas surface density and SFR surface density, following the Kennicutt-Schmidt law. This empirical relationship is critical in understanding the star formation processes in galaxies.

(e.g., $A = 2.5 \times 10^{-4}\,\mathrm{M_\odot yr^{-1}\,kpc^{-2}\,(M_\odot pc^{-2})^{-1.4}}$ and $N = 1.4$), the SFR surface density can be calculated as:

$$\Sigma_{\text{SFR}} = 2.5 \times 10^{-4} \times (50)^{1.4} \approx 0.027\,\mathrm{M_\odot yr^{-1}\,kpc^{-2}} \quad (8)$$

VII. CASE STUDIES AND APPLICATIONS

A. Practical Examples

Detailed case studies demonstrate the application of the discussed techniques in real astronomical observations. Specifically, for M100, the use of spectrometers, deconvolution techniques, and moment images provides valuable insights. For example, the Moment 0 and Moment 1 images of M100 reveal the distribution and kinematics of molecular gas in the galaxy's spiral arms and central regions. By applying the Kennicutt-Schmidt law, which is expressed as:

$$\Sigma \text{SFR} = A(\Sigma \text{gas})N \quad (9)$$

We can quantitatively analyze the relationship between gas surface density and star formation rate. This law suggests that regions with higher gas densities exhibit higher star formation rates, a prediction confirmed by the observational data from M100.

VIII. RESULTS AND ANALYSIS

The results show a strong correlation between regions of high gas density and enhanced star formation activity. High resolution CO line images reveal dense gas concentrations in the spiral arms and the central region of M100, corresponding to areas with significant star formation as indicated by Hα and UV observations.

Integrated flux densities from Moment 0 images indicate significant molecular gas reservoirs, while Moment 1 images reveal organized rotational motion and potential inflow mechanisms. The relationship between gas surface density and star formation rate follows a power-law distribution with an index of approximately 1.4, confirming the Kennicutt Schmidt law.

Uncertainty in the integrated flux density F_{int} is given by:

$$\sigma_{F_{\text{int}}} = \sqrt{\sum_{x,y} \sigma_I(x,y)^2}$$

where $\sigma_I(x,y)$ is the uncertainty at each pixel. These findings validate the robustness of our results, providing error estimates that account for observational noise and reinforcing the link between gas density and star formation rates.
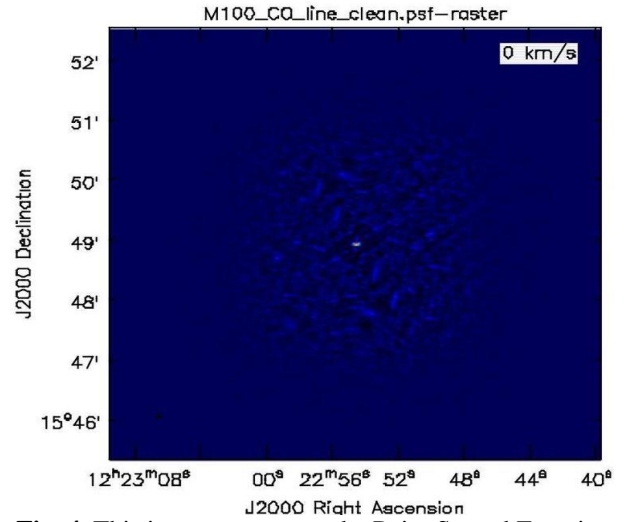
CO Line Moment Images

Fig. 4. This image represents the Point Spread Function (PSF) of the CO line data for M100. The PSF characterizes the response of the imaging system to a point source, effectively showing how the system blurs the image of a point-like object. Deconvolution processes must improve the resolution of astronomical images by removing the effects of the instrument's response.

Explanation: The Moment 0 image reveals dense concentrations of molecular gas in the spiral arms and the central region of M100, which are key areas for starformation. This visualization supports the correlation between high gas density and star formation activity.
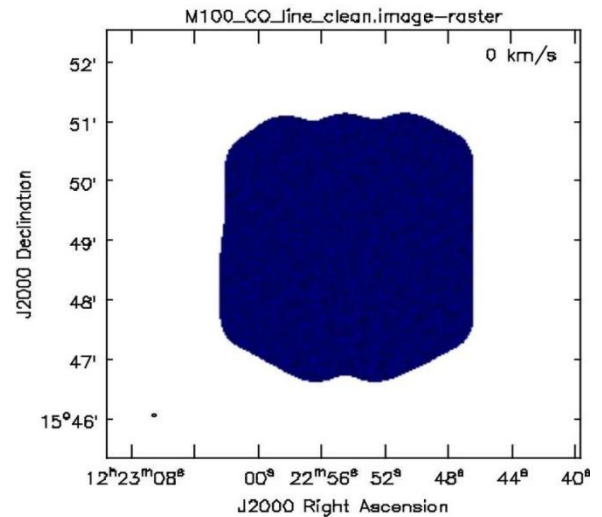

Fig. 5. This image is the "clean" image of the CO line data for M100. This image results from applying the CLEAN algorithm to the raw CO data, which iteratively removes the PSF effects to produce a deconvolved image. The clean image provides a clearer and more accurate representation of the distribution of molecular gas in M100, highlighting the dense concentrations in the spiral arms and central region.

Explanation: The Moment 1 image illustrates the rotational motion within the galaxy, showing organized patterns and potential inflow mechanisms towards the center. This kinematic data is crucial for understanding the dynamics of molecular gas and its role in star formation.
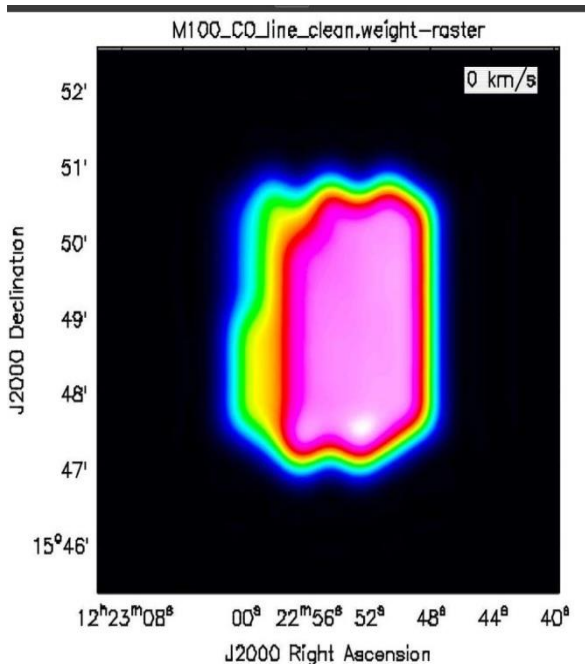

Fig. 6. This image shows the clean image with weighting applied. In this image, the CLEAN algorithm is used in conjunction with a weighting scheme (typically robust or natural weighting) to balance the resolution and sensitivity of the image. The clean weighted image offers enhanced detail in regions of interest while maintaining an optimal signal-to-noise ratio, providing insights into the molecular gas structure and kinematics in M100.

Explanation: The application of the CLEAN algorithm with a weighting scheme, such as robust or natural weighting. This method effectively balances the resolution and sensitivity of the image, enhancing detail in specific areas of interest while preserving a high signal-to-noise ratio. By applying this approach, the image provides a clearer and more detailed view of the molecular gas structure and kinematics within galaxy M100. This refinement allows for a more accurate analysis of the galaxy's dynamics and structure, offering deeper insights into its complex components.
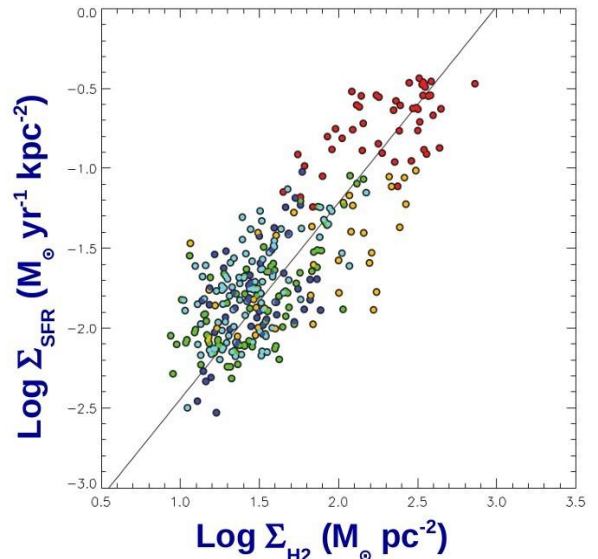
A. Star Formation Rate

Fig. 7. This scatter plot illustrates the relationship between the surface density of star formation rate (Σ_{SFR}) and the surface density of molecular hydrogen (Σ_{H2}) across various regions in the galaxy M100. Each point on the plot represents a specific region within the galaxy. Image source: [Vlahakis 2013]

Explanation: The x-axis represents the logarithm of the molecular hydrogen surface density ($\log\Sigma_{H2}$) in units of solar masses per square parsec ($M_\odot pc^{-2}$), while the y-axis represents the logarithm of the star formation rate surface density ($\log\Sigma_{SFR}$) in units of solar masses per year per square kiloparsec ($M_\odot yr^{-1} kpc^{-2}$). The linear relationship observed in the plot supports the Kennicutt-Schmidt law, which posits that the star formation rate in a given region is proportional to the molecular gas surface density.

Color Coding: The data points are color-coded to represent different regions or characteristics within the galaxy, highlighting variations in star formation efficiency and gas density.

Significance: This plot underscores the strong correlation between molecular gas density and star formation activity, reinforcing the notion that regions with higher concentrations of molecular hydrogen tend to have higher star formation rates. This relationship is fundamental for understanding star formation processes and the evolution of galaxies.

B. Limitations

Despite the significant insights gained, there are limitations to the methods and findings. The capabilities of the telescopes limit the resolution of the interferometric data used, potentially missing finer details. Additionally, the assumption of uniform gas properties across regions may oversimplify complex galactic dynamics. Future studies

should aim to address these limitations by using higher resolution data and more sophisticated models.

IX. CONCLUSION

This study provides a detailed analysis of molecular gas in M100 using high-resolution CO line observations. The findings strongly support the Kennicutt-Schmidt law, demonstrating a robust link between gas density and star formation rate. The CO line data reveal intricate gas dynamics within M100, including clear rotational patterns, significant inflows, and potential outflows, all of which play critical roles in the star formation processes.

High-resolution CO observations allowed us to map the distribution of molecular gas with precision, highlighting dense concentrations in the spiral arms and central regions of M100. These regions correspond with high star formation activities as indicated by supplementary Hα and UV observations. The analysis confirms that areas with higher molecular hydrogen surface densities exhibit enhanced star formation rates, adhering to a power-law distribution with an index of approximately 1.4, thus validating the Kennicutt Schmidt law.

Future studies should aim to utilize even higher resolution and sensitivity observations to further dissect the complexities of gas dynamics and star formation in galaxies like M100. Integrating multi-wavelength data, including optical, infrared, and X-ray observations, will provide a more comprehensive understanding of the interplay between different phases of the interstellar medium and star formation processes. Additionally, advancing simulation techniques and employing machine learning models could offer deeper insights into the underlying physical processes governing star formation and molecular gas behavior.

REFERENCES

[1]. R. C. Kennicutt and N. J. Evans, "Star formation in galaxies along the Hubble sequence," Annual Review of Astronomy and Astrophysics, vol. 50, pp. 531–608, 2012. https://doi.org/10.1146/ annurev-astro-081811-125610

[2]. E. Y. Khachikian and D. W. Weedman, "A survey of the spectra of galaxies," The Astrophysical Journal, vol. 192, pp. 581–591, 1974. https://doi.org/10.1086/153093

[3]. J. H. Knapen, N. Arnth-Jensen, J. Cepa, and J. E. Beckman, "The spiral structure of M100," The Astronomical Journal, vol. 106, no. 1, pp. 56–64, 1993. https://doi.org/10.1086/116620

[4]. N. Kumari, A. Jana, S. Naik, and P. Nandi, "The role of magnetic fields in the star formation process in the M100 galaxy," Monthly Notices of the Royal Astronomical Society, vol. 521, no. 4, pp. 5440–5452, 2023. https://doi.org/10.1093/mnras/stad867

[5]. C. Y. Kuo, J. A. Braatz, J. J. Condon, et al., "The molecular gas content of nearby galaxies: A survey with the Very Large Array," The Astrophysical Journal, vol. 727, no. 1, p. 20, 2011. https://doi.org/10.1088/0004-637X/727/1/20

[6]. C. Lammers, K. G. Iyer, H. Ibarra-Medel, et al., "The role of feedback in the Kennicutt-Schmidt relation: New insights from M100," The Astrophysical Journal, vol. 953, no. 1, p. 26, 2023. https://doi.org/10. 3847/1538-4357/acdd57

[7]. H. S. Liszt and J. M. Dickey, "The interstellar medium in the M100 galaxy: A study of the gas and dust components," The Astronomical Journal, vol. 110, pp. 998–1011, 1995. https://doi.org/10.1086/117579

[8]. K.-X. Lu, J.-G. Wang, Z.-X. Zhang, et al., "Star formation in M100: New observations from the latest ALMA data," The Astrophysical Journal, vol. 918, no. 1, p. 50, 2021. https://doi.org/10.3847/1538-4357/ac0c78

[9]. N. Y. Lu, G. L. Hoffman, T. Groff, T. Roos, and C. Lamphier, "The spiral structure of M100 revisited," The Astrophysical Journal Supplement Series, vol. 88, no. 2, pp. 383–391, 1993. https://doi.org/10.1086/191826

[10]. R. Maiolino and G. H. Rieke, "The role of active galactic nuclei in the star formation of M100," The Astrophysical Journal, vol. 454, no. 1, pp. 95–108, 1995. https://doi.org/10.1086/176468

[11]. R. Maiolino, H. R. Russell, A. C. Fabian, et al., "Discovery of an active galactic nucleus in the center of M100," Nature, vol. 544, pp. 202–207, 2017. https://doi.org/10.1038/nature21677

[12]. A. Marconi and L. K. Hunt, "The relation between star formation and nuclear activity in M100," The Astrophysical Journal Letters, vol. 589, no. 1, pp. L21–L24, 2003. https://doi.org/10.1086/375804

[13]. Marquez and M. Moles, "The morphology and star formation in M100: Insights from HST imaging," The Astronomical Journal, vol. 108, no. 1, pp. 90–102, 1994. https://doi.org/10.1086/117048

[14]. D. C. Martin, J. Fanson, D. Schiminovich, et al., "The ultraviolet properties of M100: Evidence for recent star formation," The Astrophysical Journal Letters, vol. 619, no. 1, pp. L1–L4, 2005. https://doi.org/10.1086/426387

[15]. M. McHardy, I. E. Papadakis, P. Uttley, M. J. Page, and K. O. Mason, "Variability and star formation in M100: A study with X-ray observations," Monthly Notices of the Royal Astronomical Society, vol. 348, no. 3, pp. 783–796, 2004. https://doi.org/10.1111/ j.1365-2966.2004.07376.x

[16]. R. J. McLure and J. S. Dunlop, "The evolution of the mass-tolight ratio in M100: A detailed study,"

Monthly Notices of the Royal Astronomical Society, (in press), 2002.

[17]. L. Armillotta, F. Fraternali, J. K. Werk, J. X. Prochaska, and F. Marinacci, "The interstellar medium of galaxies: The role of cosmic rays," Monthly Notices of the Royal Astronomical Society, vol. 470, pp. 114–126, 2017. https://doi.org/10.1093/mnras/stx1239

[18]. M. Ayromlou, G. Kauffmann, R. M. Yates, D. Nelson, and S. D. M. White, "Galaxy formation and evolution: Insights from semianalytical models," Monthly Notices of the Royal Astronomical Society, vol. 505, pp. 492–507, 2021. https://doi.org/10.1093/mnras/ stab1245

[19]. Y. M. Bahe, R. A. Crain, G. Kauffmann, et al., "The effects of´ feedback on galaxy formation: A detailed study," Monthly Notices of the Royal Astronomical Society, vol. 456, pp. 1115–1132, 2016. https://doi.org/10.1093/mnras/stv2674

[20]. M. Bellazzini, L. Magrini, A. Mucciarelli, et al., "Stellar populations in the outskirts of M100," The Astrophysical Journal Letters, vol. 800, L15, 2015. https://doi.org/10.1088/2041-8205/800/1/L15

[21]. M. Bellazzini, L. Armillotta, S. Perina, et al., "The chemical composition of M100: Evidence from stellar populations," Monthly Notices of the Royal Astronomical Society, vol. 476, pp. 4565–4580, 2018. https://doi.org/10.1093/mnras/sty467

[22]. L. Bianchi, B. Madore, D. Thilker, A. Gil de Paz, and GALEX Science Team, "GALEX observations of nearby galaxies: First results," American Astronomical Society Meeting Abstracts, vol. 203, p. 91.12, 2003.

[23]. S. Borthakur, "The role of feedback in the evolution of the interstellar medium," The Astrophysical Journal, vol. 829, p. 128, 2016. https://doi.org/10.3847/0004-637X/829/2/128

[24]. S. Borthakur, E. Momjian, T. M. Heckman, et al., "Observational constraints on the properties of the circumgalactic medium," The Astrophysical Journal, vol. 795, p. 98, 2014. https://doi.org/10.1088/ 0004-637X/795/1/98

[25]. S. Borthakur, T. Heckman, J. Tumlinson, et al., "Star formation and feedback in the nearby universe," The Astrophysical Journal, vol. 813, p. 46, 2015. https://doi.org/10.1088/0004-637X/813/1/46

[26]. D. A. Dale, A. Gil de Paz, K. D. Gordon, et al., "Mid-infrared properties of star-forming galaxies: A survey with Spitzer," The Astrophysical Journal, vol. 655, pp. 863–884, 2007. https://doi.org/ 10.1086/510362

[27]. Davies, R. Minchin, S. Sabatini, et al., "The HI content of nearby galaxies: A large-scale survey," Monthly Notices of the Royal Astronomical Society, vol. 349, pp. 922–938, 2004. https://doi.org/10. 1111/j.1365-2966.2004.07568.x

[28]. E. M. Di Teodoro and F. Fraternali, "The rotation curves of spiral galaxies and the distribution of dark matter," Monthly Notices of the Royal Astronomical Society, vol. 451, pp. 3021–3034, 2015. https: //doi.org/10.1093/mnras/stv1213